Available online at www.sciencedirect.com
ScienceDirect
Trans. Nonferrous Met. Soc. China 29(2019) 1211−1222
Transactions of Nonferrous Metals Society of China
www.tnmsc.cn

Microstructure and mechanical properties of as-cast Mg−8Li−*x*Zn−*y*Gd (*x*=1, 2, 3, 4; *y*=1, 2) alloys

Si-jie OUYANG[1,2], Wen-cai LIU[1,2], Guo-hua WU[1,2], Hao JI[1,2], Zhan-kui GAO[1,2], Xiang PENG[1,2], Zhong-quan LI[3,4], Wen-jiang DING[1,2]

1. National Engineering Research Center of Light Alloy Net Forming and Key State Laboratory of Metal Matrix Composite, School of Materials Science and Engineering, Shanghai Jiao Tong University, Shanghai 200240, China;
2. Shanghai Innovation Institute for Materials, Shanghai 200444, China;
3. Shanghai Spaceflight Precision Machinery Institute, Shanghai 201600, China;
4. Shanghai Engineering Technology Research Center of Near-Net-Shape Forming for Metallic Materials, Shanghai 201600, China

Received 31 August 2018; accepted 17 December 2018

Abstract: The as-cast Mg−8Li−*x*Zn−*y*Gd (*x*=1, 2, 3, 4; *y*=1, 2; wt.%) alloys were prepared in a vacuum induction furnace and their microstructure and mechanical properties were investigated. The results show that the increase of Zn content results in the volume fraction of *W*-phase ($Mg_3Zn_3Gd_2$) increasing while that of Mg_3Gd phase decreasing. The strength of Mg−8Li−*x*Zn−1Gd alloys is improved with the increase of Zn content, which is ascribed to the second phase strengthening of fine strip-like *W*-phase and the solid solution strengthening of Zn element. For Mg−8Li−4Zn−*y*Gd alloys, the increase of Gd content leads to the appearance of coarse and discontinuous net-like *W*-phase, which decreases the strength. The Mg−8Li−4Zn−1Gd alloy exhibits an optimum comprehensive performance with the yield strength, ultimate tensile strength and elongation of 154.7 MPa, 197.0 MPa and 12.4%, respectively. In addition, the aging behavior of the typical alloys was also investigated.

Key words: Mg−Li−Zn−Gd alloy; *W*-phase; microstructure; mechanical properties; aging behavior

1 Introduction

Due to the outstanding performance, especially high specific strength, good damping property and electromagnetic screen capacity, Mg alloys attract more and more attention over the years. Moreover, magnesium alloys have a wide range of application in aerospace, automobile and electronics industry [1−5]. However, most of conventional Mg alloys with hexagonal close-packed (hcp) structure exhibit a poor ductility because there exist only one slip plane and three slip systems at room temperature [6,7]. Alloying magnesium with lithium (Li), by transferring hcp structure to bcc (body-centered cubic) structure, which contributes to more slip systems, can enhance the deformability of Mg alloys. Furthermore, the addition of Li with very low density of 0.53 g/cm^3 can decrease the density of magnesium alloys from ~1.8 to 1.25−1.65 g/cm^3 [5,8]. However, there are some disadvantages in Mg−Li alloys such as relatively poor strength, low corrosion resistance and aging softening phenomenon [9], which deeply restrict the wide application as engineering structure materials. Alloying is the main effective and simple method to overcome this drawback [10].

The main strengthening alloying elements are Al and Zn in Mg−Li alloys. Al element can effectively improve the strength of Mg−Li alloys but simultaneously damage the plasticity [11]. Zn element can not only enhance the strength of Mg−Li alloys but also have little

Foundation item: Project (2016YFB0301004) supported by the National Key Research and Development Program of China; Project (51771115) supported by the National Natural Science Foundation of China; Project (6141B06310106) supported by the Joint Fund for Space Science and Technology, China; Project (009-031-001) supported by the Science and Technology Innovation Program, China; Project (USCAST2016-18) supported by the Research Program of Joint Research Center of Advanced Spaceflight Technologies, China; Project (SAST2016048) supported by the Science Innovation Foundation of Shanghai Academy of Spaceflight Technology, China

Corresponding authors: Wen-cai LIU, Tel: +86-21-54742630, Fax: +86-21-34202794, E-mail: liuwc@sjtu.edu.cn; Guo-hua WU, E-mail: ghwu@sjtu.edu.cn

DOI: 10.1016/S1003-6326(19)65028-4

bad effect on the plasticity. In traditional Mg−Zn−RE alloys [3,12], the formation of complex Mg−Zn−RE ternary phases contributes to excellent mechanical properties. Similarly, the addition of Zn and RE into Mg−Li alloys, including Y, Gd, Er, etc, can help to overcome the deficiency of poor strength. The former study [13] indicated that the coexistence of *W*-phase and Mg_3Gd phase plays an important role in the second phase strengthening in the as-cast Mg−Zn−Gd alloy. It has been reported [14] that the volume fraction of *W*-phase increases with increasing the addition of Zn in Mg−8Gd−*x*Zn−0.4Zr alloys. Therefore, the literatures provided a thought of investigating the effect of Zn content in as-cast Mg−Li−RE alloys and improving the strength of Mg−Li alloys by forming the strengthening *W*-phase. Present work aims to explore the microstructure evolution associated with different Zn and Gd contents in the as-cast Mg−Li alloys and analyze the corresponding strengthening mechanisms. Aging softening phenomenon is frequently reported [4,5,15], which limits the application widely. The aging behavior of the investigated alloys will be explored, which can provide a guide for resistance to aging softening.

In this work, Mg−8Li (wt.%) was selected as the based material, in which there existed duplex structure with high strength and good plasticity. Zn and Gd were chosen as alloying elements to improve the strength of Mg−8Li alloys. Mg−8Li−*x*Zn−1Gd (*x*=1, 2, 3, 4, wt.%, named as LZG alloy) alloys were designed in order to investigate the influence of Zn content on microstructure and tensile properties. Mg−8Li−4Zn−*y*Gd (*y*=1, 2, wt.%) alloys were designed for the purpose of further exploring the effect of Gd addition on microstructure and tensile properties. The reinforcement mechanism was analyzed and discussed on the basis of microstructure characteristic. In addition, the aging curves of Mg−8Li−3Zn−1Gd and Mg−8Li−4Zn−1Gd alloy were given to demonstrate the aging behavior of Mg−Li−Zn−Gd alloys.

2 Experimental

Mg−Li−Zn−Gd alloys were prepared with commercial pure (CP) magnesium (99.98 wt.%), zinc (99.96 wt.%), lithium (99.98 wt.%) and Mg−30wt.%Gd master alloy. Raw materials by calculated masses were melted in a stainless crucible of the vacuum induction melting furnace with argon acting as the protected gas. After the raw materials were melted, the melt was stirred to make the melt homogeneous with electromagnetic agitation for 3 min, kept for 10 min and then flowed into a metal mold preheated to 200 °C to cast ingots. For the purpose of investigating the aging behavior of Mg−Li−Zn−Gd alloys, solid solution treated (350 °C, 4 h) and as-cast [16] Mg−8Li−3Zn−1Gd and Mg−8Li−4Zn−1Gd alloys were aging treated at 75 and 125 °C.

The chemical compositions of the investigated alloys are listed in Table 1, which was analyzed by inductively coupled plasma-atomic emission spectrometry (ICP, Perkin Elmer). The actual composition is relatively close to the nominal composition. The microstructure samples of the alloys were made by standard metallographic procedures. After being polished and etched with 4 vol.% nitric acid alcohol solution, the metallographic observation was conducted by optical microscope (OM, ZEISS). In addition, the clearly detailed morphology was observed by scanning electron microscope (SEM, PHENOM XL), which was equipped with the energy dispersive spectrometer (EDS). The fracture surface was observed by SEM. The samples for transmission electron microscope (TEM) observation were made by mechanically thinning to ~80 μm and subsequently processed by argon ion milling (Gatan 691). TEM observation was carried out by JEM−2100 at 200 kV equipped with selected area electron diffraction (SAED).

Table 1 Chemical compositions of Mg−8Li−*x*Zn-*y*Gd (*x*=1, 2, 3, 4; *y*=1, 2; wt.%) alloys

Alloy	Nominal composition	Zn/Gd ratio	Actual composition/wt.%			
			Li	Zn	Gd	Mg
LZG811	Mg−8Li−1Zn−1Gd	1	8.5	1.1	1.1	Bal.
LZG821	Mg−8Li−2Zn−1Gd	2	8.7	2.0	1.1	Bal.
LZG831	Mg−8Li−3Zn−1Gd	3	7.2	2.5	0.7	Bal.
LZG841	Mg−8Li−4Zn−1Gd	4	8.2	4.0	1.0	Bal.
LZG842	Mg−8Li−4Zn−2Gd	2	8.3	3.5	2.3	Bal.

The phase compositions of Mg−Li−Zn−Gd alloys were identified by X-ray diffraction (XRD, Rigaku) with the radiation resource of Cu K_α, at the step size of 0.02° and scanning rate of 4 (°)/min. The volume fractions of second phases were measured by quantitative graphic analysis software. The Vickers hardness (HV) of the alloys was measured at ambient temperature by loading of 49 N and holding for 15 s. The density of the alloys was acquired by the Archimedes method. Specimens for tensile tests were machined into rectangle with gauge size of 15 mm × 3 mm × 2 mm by the electric spark erosion machine. The room-temperature tensile tests were conducted at the rate of 1.0 mm/s on the Zwick/Roell Z020 tensile test machine equipped with an extensometer.

3 Results and discussion

3.1 Microstructure

Optical microstructures of as-cast Mg−8Li−*x*Zn−

*y*Gd (*x*=1, 2, 3, 4; *y*=1, 2; wt.%) alloys are shown in Fig. 1. As presented in Figs. 1(a−e), as-cast Mg−8Li−*x*Zn−*y*Gd alloys display typical duplex structure, which consists of the gray *β*-Li phase and white *α*-Mg phase. The shapes of *α*-Mg phase are long needle-like and short rod-like. For Mg−8Li−*x*Zn−1Gd (*x*=1, 2, 3, 4, wt.%), with the content of Zn increasing, the amount of the short rod-like *α*-Mg decreases and that of the long needle-like *α*-Mg increases, which is indicated in Figs. 1(a−d). As shown in Figs. 1(d, e), with the addition of Gd, the appearance of second phases transforms from particle-like into net-like and the reticular regions coarsen. With the increase of Zn and Gd content, the average sizes of *α*-Mg grain for all of the investigated alloys are in the same order of magnitude. Table 2 presents the volume fractions of precipitates in the investigated alloys. The result indicates that the volume fraction of precipitates in Mg−8Li−*x*Zn−1Gd (*x*=1, 2, 3, 4, wt.%) slightly increases with the increase of Zn content, from 1.7 vol.% in LZG811 alloy to 4.5 vol.% in LZG841 alloy. However, with the addition of Gd in LZG841, the volume fraction of second phases in the alloys significantly increases, from 4.5 vol.% in LZG841 alloy to 6.9 vol.% in LZG842 alloy.

In order to identify the detailed phase constitution of Mg−8Li−*x*Zn−*y*Gd alloys, the XRD patterns of investigated alloys are shown in Fig. 2. It is demonstrated that the as-cast Mg−8Li−*x*Zn−*y*Gd alloys mainly consist of *α*-Mg, *β*-Li, *W*-phase, Mg−Li−Zn and Mg_3Gd phase. With the increase of Zn content, the intensity of diffraction peaks of *W*-phase (face-centered cubic structure) increases. The diffraction peaks of Mg_3Gd phase in LZG811 alloy exhibit the highest intensity and those in LZG842 alloy present the lowest. Literature [17] reported that the diffraction peaks of *W*-phase presented some degree shift in XRD patterns because the lattice parameter of *W*-phase was variable with the alteration of Zn/Gd ratio. However, in this work, the diffraction peaks of *W*-phase for the alloys with different Zn/Gd ratios are in the same degree. So, the lattice parameter of *W*-phase is invariable, which is inconsistent with that in Mg−Zn−Gd alloys.

Figure 3 displays the SEM micrographs of the investigated alloys, which aims to illustrate the morphology of various second phases in Mg−8Li−*x*Zn−*y*Gd alloys. It is shown that the Mg−8Li−*x*Zn−*y*Gd

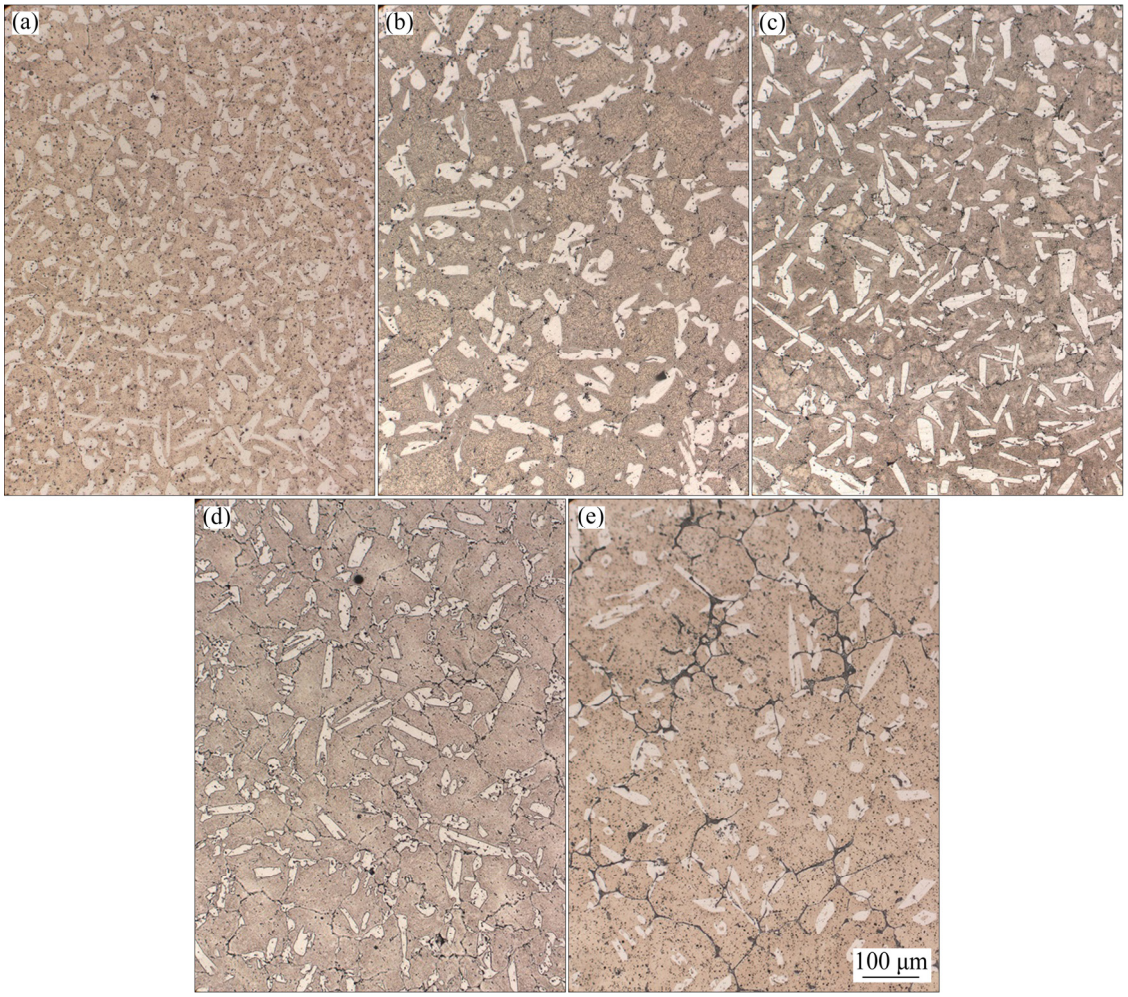

Fig. 1 Optical microstructures of Mg−8Li−*x*Zn−*y*Gd alloys: (a) *x*=1, *y*=1; (b) *x*=2, *y*=1; (c) *x*=3, *y*=1; (d) *x*=4, *y*=1; (e) *x*=4, *y*=2

Table 2 Volume fractions of precipitates in Mg−8Li−*x*Zn−*y*Gd (*x*=1, 2, 3, 4; *y*=1, 2; wt.%) alloys

Alloy	Volume fraction of precipitates/%
LZG811	1.7±0.2
LZG821	2.3±0.2
LZG831	3.2±0.5
LZG841	4.5±0.6

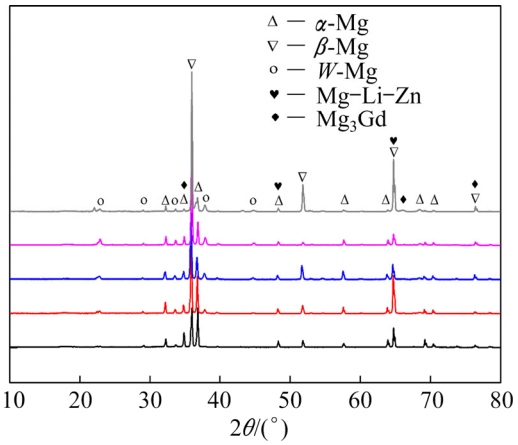

Fig. 2 XRD patterns of Mg−8Li−*x*Zn−*y*Gd (*x*=1, 2, 3, 4; *y*=1, 2; wt.%) alloys

alloys exhibit a typically dendritic microstructure. The strip-like phases mainly distributing in the matrix are *W*-phase. With the increase of Zn content, the amount of *W*-phase gradually increases, as shown in Figs. 3(a−d). The addition of Gd element leads to coarsening of *W*-phase and formation of discontinuous netlike structure, as presented in Figs. 3(d, e). It could also be seen that the eutectic phase appears near the network *W*-phase. The eutectic phase could be *I*-phase and the coexistence of *I*-phase and *W*-phase in Mg−Li−Zn−RE alloys is observed, which is similar with Ref. [2]. Previous researches [4] indicated that with the increase of Zn and Gd contents, the grains of as-cast Mg−Li−Zn−Gd alloys were refined gradually. This suggests that Gd can change solubility of Zn, which decreases the solidus curve and shortens the time for nucleation, and then reduces the grain size [18]. In present work, some Gd elements exist in the form of *W*-phase. However, with the increase of Gd content, the netlike microstructure is remarkably coarsened by the increase *W*-phase fraction, which greatly weakens the grain refining effect of element Gd. Therefore, with Gd content increasing, the average grain sizes of the alloys are basically the same.

Figure 4 presents EDS map scanning results of Mg, Zn and Gd elements in LZG841 alloy. Mg element dispersively distributes in the matrix and is relatively poor in the netlike phase, as seen in Fig. 4(b). As revealed in Fig. 4(c), most of Zn elements concentrate in the coarse reticular phases, namely *W*-phase. The other Zn elements distributes uniformly in the matrix and exist in the form of solid solution. As illustrated in Fig. 4(d), the distribution of Gd element is extremely similar to that of Mg element. The EDS point scanning results of the four sites marked in Fig. 4 are listed in Table 3. The Zn content of the sites in the netlike second phase is more

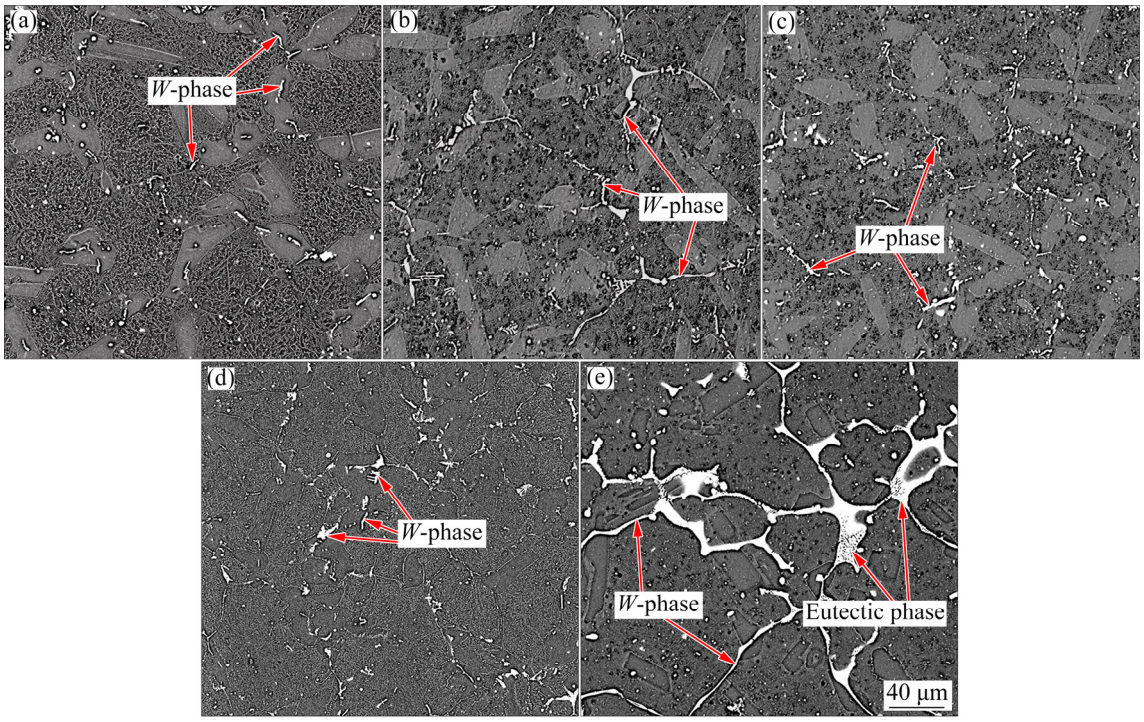

Fig. 3 SEM micrographs of Mg−8Li−*x*Zn−*y*Gd alloys: (a) *x*=1, *y*=1; (b) *x*=2, *y*=1; (c) *x*=3, *y*=1; (d) *x*=4, *y*=1; (e) *x*=4, *y*=2

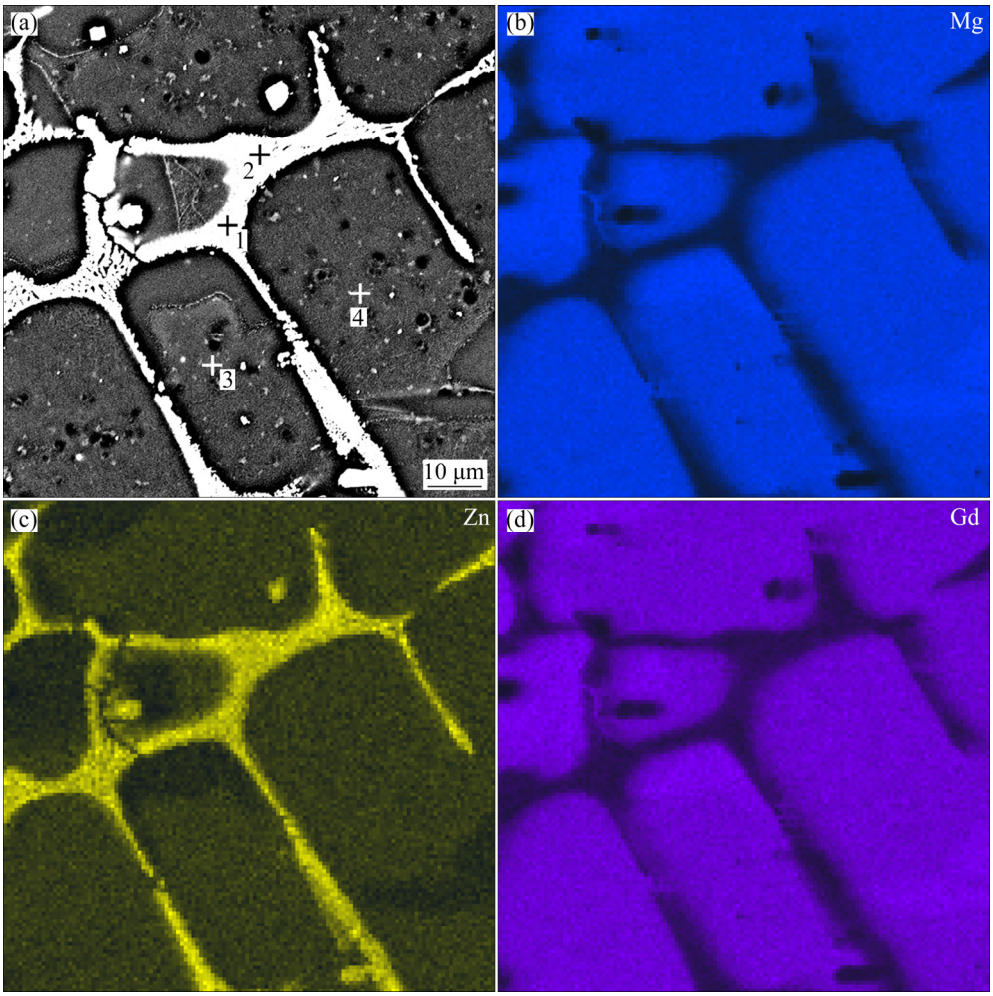

Fig. 4 EDS map scanning results of Mg−8Li−4Zn−1Gd alloy

Table 3 EDS point scanning results of Mg−8Li−4Zn−1Gd alloy in Fig. 4 (at.%)

Position	Mg	Zn	Gd
1	89.34	7.07	3.59
2	90.89	6.53	2.58
3	91.94	0.84	7.22
4	94.47	0.58	4.95

than that in the matrix. The Gd content of the sites in the matrix is more than that in the net-like second phase. The point scanning results are consistent with the mapping results. The EDS map and point scanning results indicate that most of Gd atoms have been dissolved into matrix, accompanied by the formation of some Gd-containing second phases within matrix.

Figure 5 shows the typical SEM images in large magnification and Table 4 gives the EDS analysis results of Mg−8Li−*x*Zn−*y*Gd alloy in Fig. 5, which are combined to identify the major phase in Mg−8Li−*x*Zn−*y*Gd alloys. The *α*-Mg phase and *β*-Li phase are labeled in the image. The block-like phases (labeled as A) locate in *α*-Mg and *β*-Li matrix, with the molar ratio of Mg to Gd close to 3, which are identified as Mg_3Gd phase. The strip-like phases (labeled as B) distribute at *α*-Mg/*β*-Li phase interface and within *α*-Mg matrix. EDS point scanning of point B indicates that the molar ratio of Zn to Gd is close to 1.5, identified as *W*-phase ($Mg_3Zn_3Gd_2$). The Mg−Li−Zn phase cannot be determined because the energy of Li element is too low to distinguish by EDS analysis. For LZG821, LZG831 and LZG841 alloys, the amount of block-like Mg_3Gd phase apparently decreases while that of the strip-like *W*-phase significantly increases. The result is consistent with the XRD pattern. The electronegativities of Mg, Zn and Gd are 1.3, 1.6 and 1.2, respectively. The electronegativity difference between Zn and Gd is larger than that between Mg and Gd. So, Gd prefers to combine with Zn to form *W*-phase. With the addition of Zn, more Gd elements are used to form *W*-phase ($Mg_3Zn_3Gd_2$), and less Gd elements are left to form Mg_3Gd phase, which contributes to the increase of *W*-phase amount and the decrease of Mg_3Gd phase amount.

The TEM observation and corresponding selected-

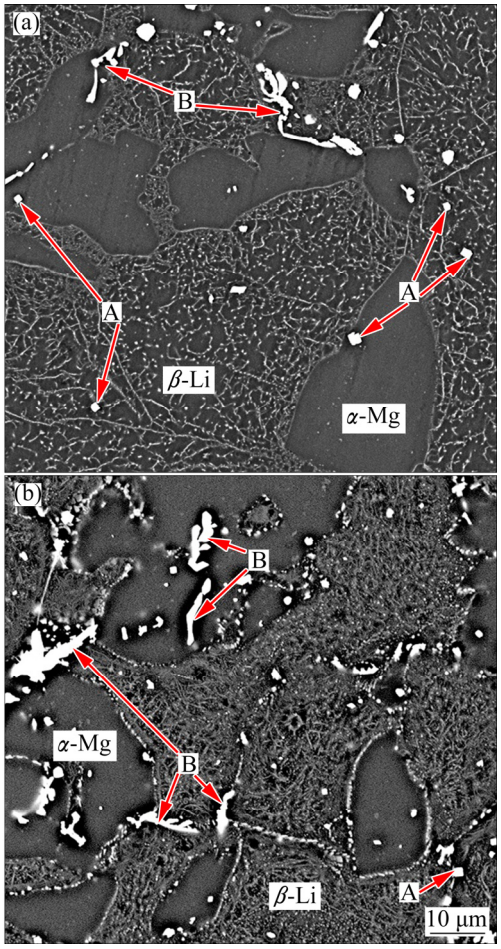

Fig. 5 Typical SEM images of Mg−8Li−*x*Zn−*y*Gd alloys: (a) LZG821 alloy; (b) LZG841 alloy

Table 4 EDS point results of Mg−8Li−4Zn−1Gd alloy in Fig. 5 (at.%)

Position	Mg	Zn	Gd	Phase composition
A	74.5	−	25.5	Mg_3Gd
B	70.0	17.8	12.2	$Mg_3Zn_3Gd_2$
Matrix	94.5	0.8	4.7	*α*-Mg

area electron diffraction (SAED) patterns for LZG841 alloy are shown in Fig. 6. The matrix *α*-Mg is labeled in Fig. 6(a) with the hcp structure and the corresponding SAED patterns with a zonal axis of $[1\bar{2}1\bar{3}]$. The black elliptic phase A in Fig. 6(b) is considered as *W*-phase (fcc structure) with a zonal axis of [011], the lattice parameter of a=0.79 nm and chemical composition of 56.80 at.% Mg, 23.34 at.% Zn and 19.86 at.% Gd. As reported by LIU et al [19], *W*-phase is partially ordered $AlMnCu_2$-type fcc structure with a lattice parameter of a=0.768 nm and composition of 31.21 at.% Mg, 43.05 at.% Zn and 25.74 at.% Gd. The morphology of gray strip-like B is shown in Fig. 6(c), which is considered as Li_2MgZn with a zonal axis of [001], because the lattice parameter of phase B is calculated as a=0.60 nm, which is close to the standard value of 0.62 nm in PDF card 2004. The morphology of black polygonous phase C is shown in Fig. 6(d), which is identified as Mg_3Gd with a zonal axis of [001]. The pattern of *I*-phase was not found in this work because the quantity of *I*-phase was very little.

3.2 Mechanical properties

The density, hardness and tensile properties of the Mg−8Li−*x*Zn−*y*Gd alloys are listed in Table 5. As shown in Table 5, the density of Mg−Li alloys increases slightly with the addition of Zn and Gd elements. All of the studied alloys are in the very low density, less than 1.6 g/cm^3. LZG842 alloy has the maximum density of 1.59 g/cm^3 among the investigated alloys, which is 8.3% lower than that of pure magnesium alloys. In the Mg−8Li−*x*Zn−1Gd (x=1, 2, 3, 4, wt.%) alloys, with the increase of Zn content, the hardness gradually increases, which is due to the increase of Zn-containing phase (most of these phases are more effectively hardened than *α*-Mg [2]). When adding Gd in LZG841, the hardness decreases slightly, maybe owing to the increase of the Gd-containing phase. The tensile properties of the Mg−8Li−*x*Zn−*y*Gd alloys are demonstrated in Fig. 7. Typical strain−stress curves of the investigated alloys are illustrated in Fig. 8. The yield strength (YS) and ultimate tensile strength (UTS) are improved with the increase of Zn content in the Mg−8Li−*x*Zn−1Gd alloys. When adding Gd in LZG841 alloy, the YS and UTS decrease. In addition, with the Zn content increasing, the elongation is improved significantly, but further increasing Zn content results in the reduction of elongation. The maximal YS and UTS simultaneously appear in the Zn/Gd ratio of 4 and the optimal elongation appears in the Zn/Gd ratio of 3. In summary, LZG841 alloy exhibits an optimal combination of tensile properties with the YS, UTS and elongation of 154.7MPa, 197.0 MPa and 12.4%, respectively. The YS and UTS of LZG841 alloy are improved by about 56.9% and 39.2% compared with those of LZG811 alloy (98.6 MPa and 141.5 MPa), respectively.

The strengthening mechanisms in Mg−Li alloys may come from second phase strengthening, fine-grain strengthening, solid solution strengthening and work hardening [6,20−22]. In this study, the average grain sizes of the alloys are unchangeable on the whole and the investigated alloys are in as-cast state. Therefore, the major reinforcing mechanisms include solid solution strengthening and second phase strengthening.

It has been reported that the broken and fine *W*-phases contribute to the dispersion strengthening of the Mg−Zn−Er alloys, and the strength of alloys rises with the increase of the volume fraction of the *W*-phase [1]. Fine *W*-phase particles have an effective

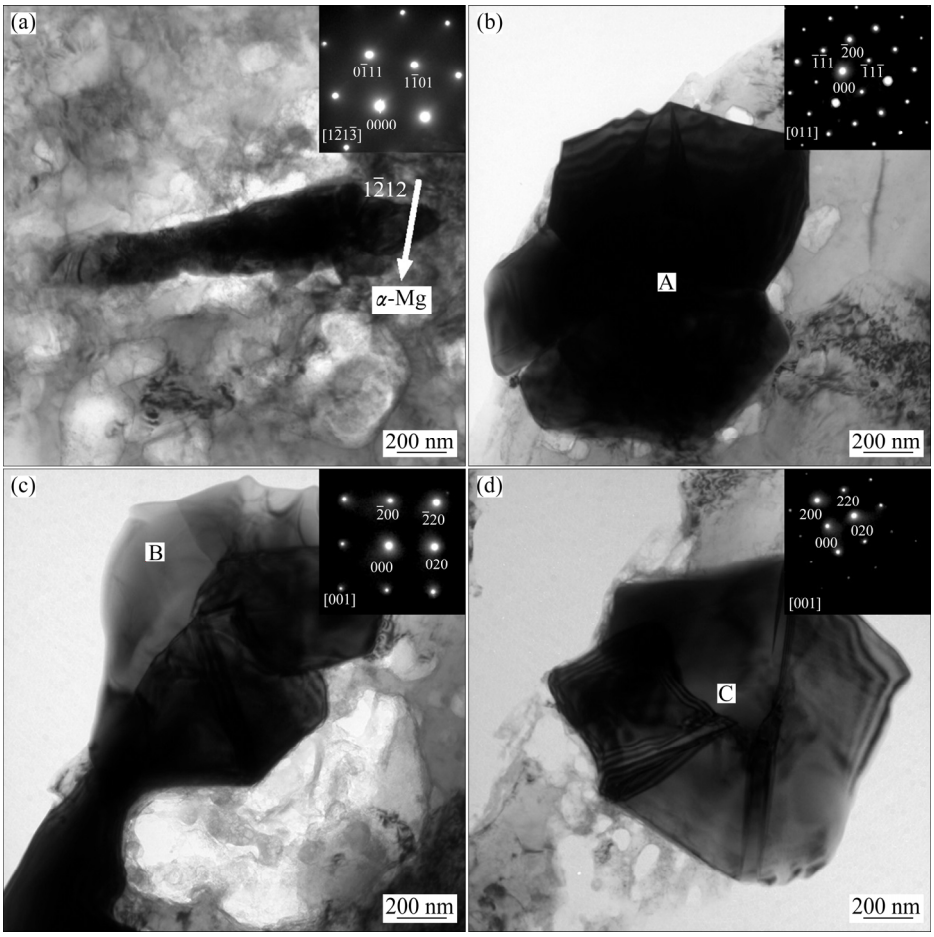

Fig. 6 TEM images of Mg−8Li−4Zn−1Gd alloy and corresponding SAED patterns

Table 5 Mechanical properties of Mg−8Li−*x*Zn−*y*Gd (*x*=1, 2, 3, 4; *y*=1, 2; wt.%) alloys

Alloy	Mechanical properties				
	Density/(g·cm^{-3})	Hardness (HV)	YS/MPa	UTS/MPa	Elongation/%
Mg−8Li−1Zn−1Gd	1.54	55.1	98.6	141.5	21.8
Mg−8Li−2Zn−1Gd	1.55	61.1	112.8	151.3	28.4
Mg−8Li−3Zn−1Gd	1.57	68.9	129.3	176.0	33.0
Mg−8Li−4Zn−1Gd	1.59	83.0	154.7	197.0	12.4
Mg−8Li−4Zn−2Gd	1.59	72.2	136.3	165.0	19.0

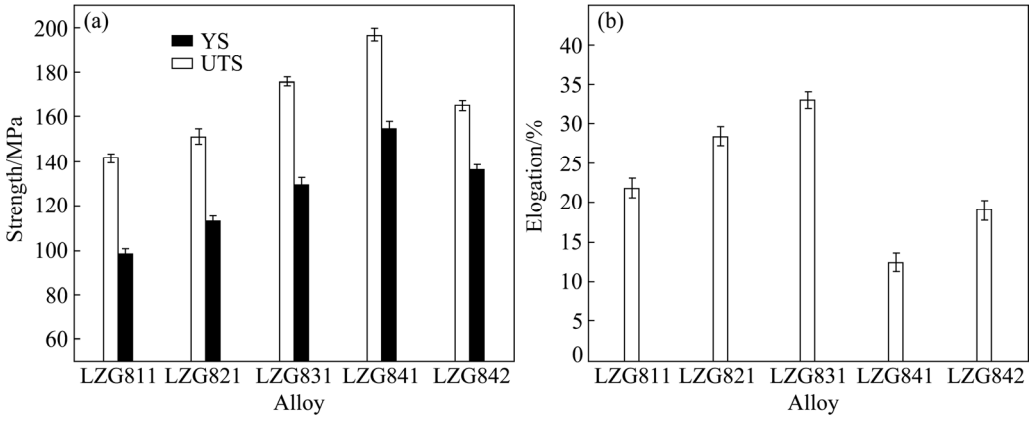

Fig. 7 Tensile properties of Mg−8Li−*x*Zn−*y*Gd (*x*=1, 2, 3, 4; *y*=1, 2; wt.%) alloys

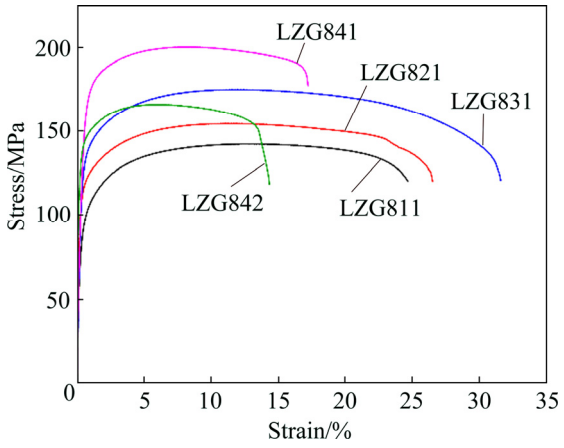

Fig. 8 Tensile strain−stress curves of Mg−8Li−*x*Zn−*y*Gd (*x*=1, 2, 3, 4; *y*=1, 2; wt.%) alloys

strengthening effect on Mg−Li alloys because fine *W*-phase particles have strong pinning effect on grain boundaries and retard the dislocation movement during the deformation process. In addition, due to the fcc structure of *W*-phase and the incoherency between *W*-phase and matrix, *W*-phase is harmful to the ductility. Mg_3Gd phase with BiF_3-type fcc structure formed due to non-equilibrium solidification during the casting process [23]. It has been reported [24] that Mg_3Gd phase is a main strengthening phase for Mg−9Li−5Gd−1Zr alloys. Mg_3Gd phase is a fine quadrangular phase, which is good to strength and harmful to ductility.

The effect of Zn and Gd on tensile properties of the Mg−8Li−*x*Zn−*y*Gd alloys can be explained as follows. Firstly, the volume fraction of Mg_3Gd phase decreases with the increase of Zn content, which results in the decrease of second phase strengthening effect. However, the volume fraction of *W*-phase increases as the content of Zn increases, which contributes to the improved strength of Mg−Li alloys. The effect of *W*-phase is higher than that of Mg_3Gd phase [13]. In this work, the volume fraction of *W*-phase is obviously more than that of Mg_3Gd phase. Therefore, the increase of strength from the *W*-phase increasing is more than the decrease of strength from Mg_3Gd phase decreasing. Secondly, with the increase of Zn content, the solid solution strengthening effect of Zn increases. Zn is one of important solid solution elements used in Mg alloys because both of Zn and Mg have hcp structure. It is indicated that the solubility of Zn atoms in the matrix for LZG841 alloy is in the range of 0.5−0.9 at.% (1.2−1.6 wt.%). Thus, solid solution strengthening is more and more important for the improvement of strength with the addition of Zn and Gd. Thirdly, with the content of Gd increasing, the strip-like *W*-phase starts to coarsen and turn into network severely. The stress concentration occurs more easily in the large net-like *W*-phase and the strengthening effect of *W*-phase for LZG842 alloys is vastly impaired. Therefore, LZG841 alloy has the maximum YS and UTS among the investigated alloys. Because of the outstanding ductility of *β*-Li, the negative impact of *W*-phase on ductility can be counteracted by the coordinating deformation of two phases [4]. All of the studied Mg−Li−Zn−Gd alloys show excellent ductility in the tensile test. Both Mg_3Gd phase and *W*-phase are harmful to the ductility of Mg−8Li−*x*Zn−*y*Gd alloys, demonstrated in the fracture surface analysis. For Mg−8Li−*x*Zn−1Gd alloys, the amount of Mg_3Gd phase decreases while that of *W*-phase increases. When the ductility increase (reduction of Mg_3Gd phase) is equal to ductility decrease (augment of *W*-phase), LZG831 alloy displays the maximal elongation. LZG842 alloy has a higher elongation than LZG841 alloy possibly due to the existence of *I*-phase in LZG842 alloy.

Figure 9 demonstrates the fractomorphologies of tensile samples of Mg−8Li−*x*Zn−*y*Gd alloys acquired by SEM. As illustrated in Figs. 9(a−c, e), it is obvious that typical ductile fracture mode presents on the fracture surface. The fracture surfaces of LZG831 consist of the smallest and deepest dimples in Fig. 9(c), which indicates that the LZG831 has the optimal ductility, while that of LZG842 consists of big and shallow dimples in Fig. 9(e). As shown in Fig. 9(d), the as-cast fracture surface is composed of tear ridges, cleavage planes and few dimples, which indicates the mixture of brittle and ductile fracture. Therefore, LZG841 has the poorest plasticity. The fractograph is in consistent with the elongation results shown in the mechanical properties of Mg−8Li−*x*Zn−*y*Gd alloys.

The results of EDS point scanning present that the particle A in Fig. 9(c) is made up of 78.9% Mg and 21.1% Gd, with the Mg/Gd of 3 in molar ratio. Combined with XRD patterns, the particle is identified as Mg_3Gd. The EDS point scanning result of particle B in Fig. 9(b) (84.06% Mg, 9.08% Zn, 6.86% Gd) presents that the Zn/Gd ratio in molar ratio is about 1.32, which might be judged for *W*-phase ($Mg_3Zn_3Gd_2$). It is deduced that *W*-phase and Mg_3Gd in the dimples, as hard and brittle phases, can be the source of crack and cracks initiate in the interface of the matrix/*W*-phase (matrix/Mg_3Gd).

3.3 Aging behavior of LZG831 and LZG841

Aging behavior of as-cast and solution-treated (350 °C, 4 h) LZG831 and LZG841 alloys with aging treatment at 75 and 125 °C is illustrated in Fig. 10. The hardness of aging at 125 °C is less than that of aging at 75 °C. The aging curves of the studied alloys at 125 °C are similar to those at 75 °C, and they arrive peak aging at the same time (4 h). The previous study indicated that

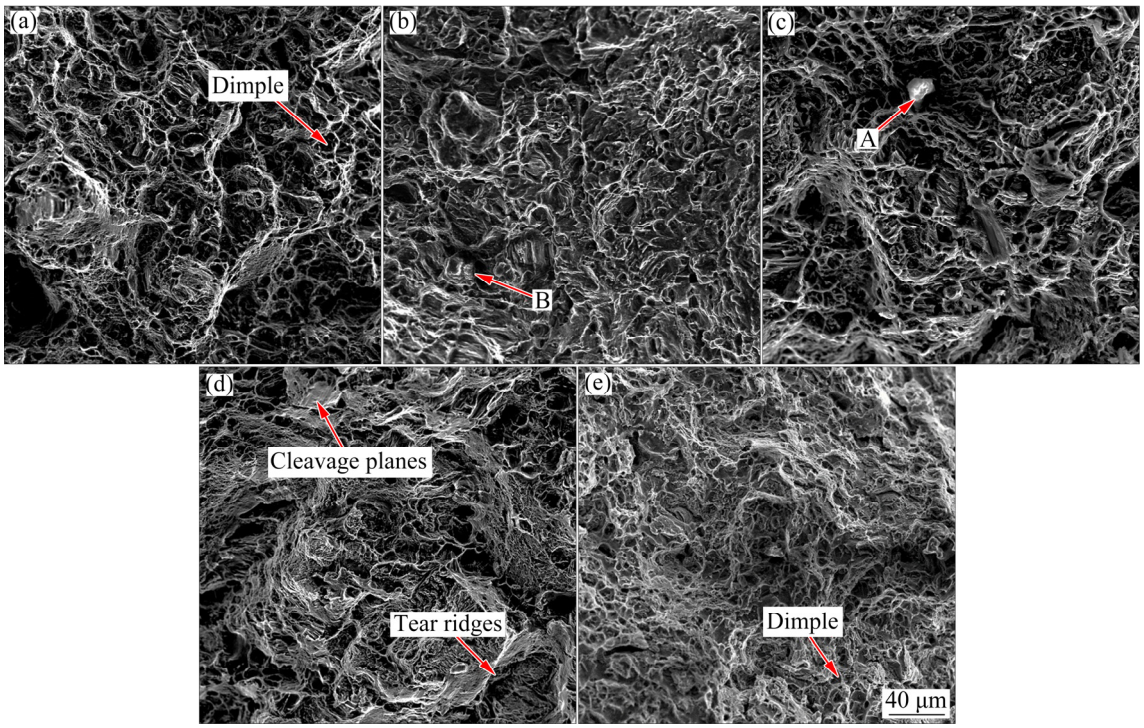

Fig. 9 Fractographs of tensile tested samples of Mg−8Li−*x*Zn−*y*Gd alloys: (a) *x*=1, *y*=1; (b) *x*=2, *y*=1; (c) *x*=3, *y*=1; (d) *x*=4, *y*=1; (e) *x*=4, *y*=2

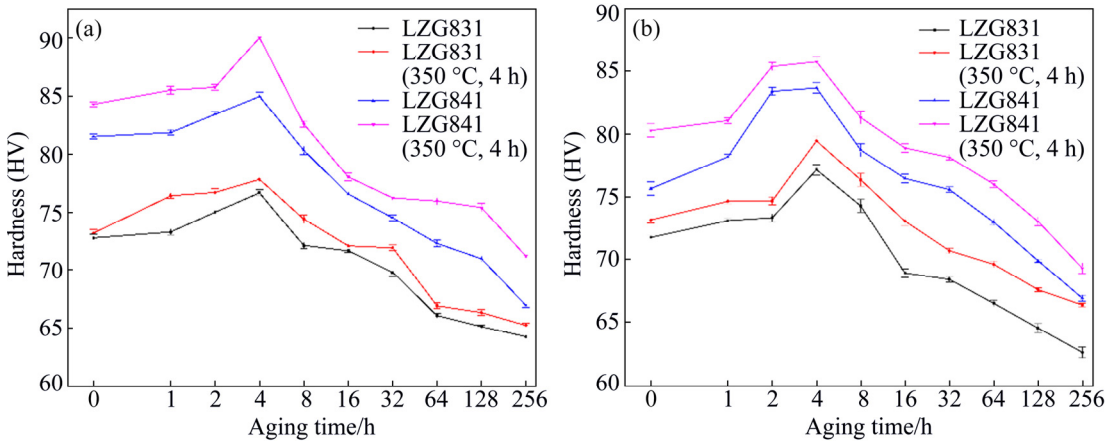

Fig. 10 Aging behavior of as-cast or solution-treated (350 °C, 4 h) LZG831 and LZG841alloys at different aging temperatures: (a) 75 °C; (b) 125 °C

the hardness of Mg−Li−Al alloys reached the maximum values at aging time around 5 h and then decreased with longer aging time [25].

With the addition of Zn element, Mg−Li alloys can be strengthened by Li_2MgZn phase. However, Li_2MgZn, as a metastable phase, will decompose into LiMgZn phase at high temperature [26]. Since *W*-phase is a thermostable phase [27], the hardening and softening effects of Mg−Li−Zn−Gd alloys are basically determined by the evolution of Mg−Li−Zn phase [25]. It can be seen that with the aging time increasing, the hardness of the alloys increases in the first stage and then decreases in the second stage. The metastable phase Li_2MgZn forms in the early aging stage, which is detected in the TEM observation. Then, in the later aging stage, the metastable Li_2MgZn phase is decomposed into LiMgZn phase. In addition, with the aging time increasing, second phases aggregate and weaken both solid solution strengthening and the precipitate hardening [16]. With the increase of aging temperature, the transformation and aggregation of second phases accelerate, which weakens the effect of precipitate hardening. Therefore, the hardness of the alloys aged at 125 °C is less than that of the alloys aged at 75 °C. The microstructures at different aging time demonstrated in Fig. 11 are in agreement with the above analysis, and the β-Li phase becomes dark as a result of

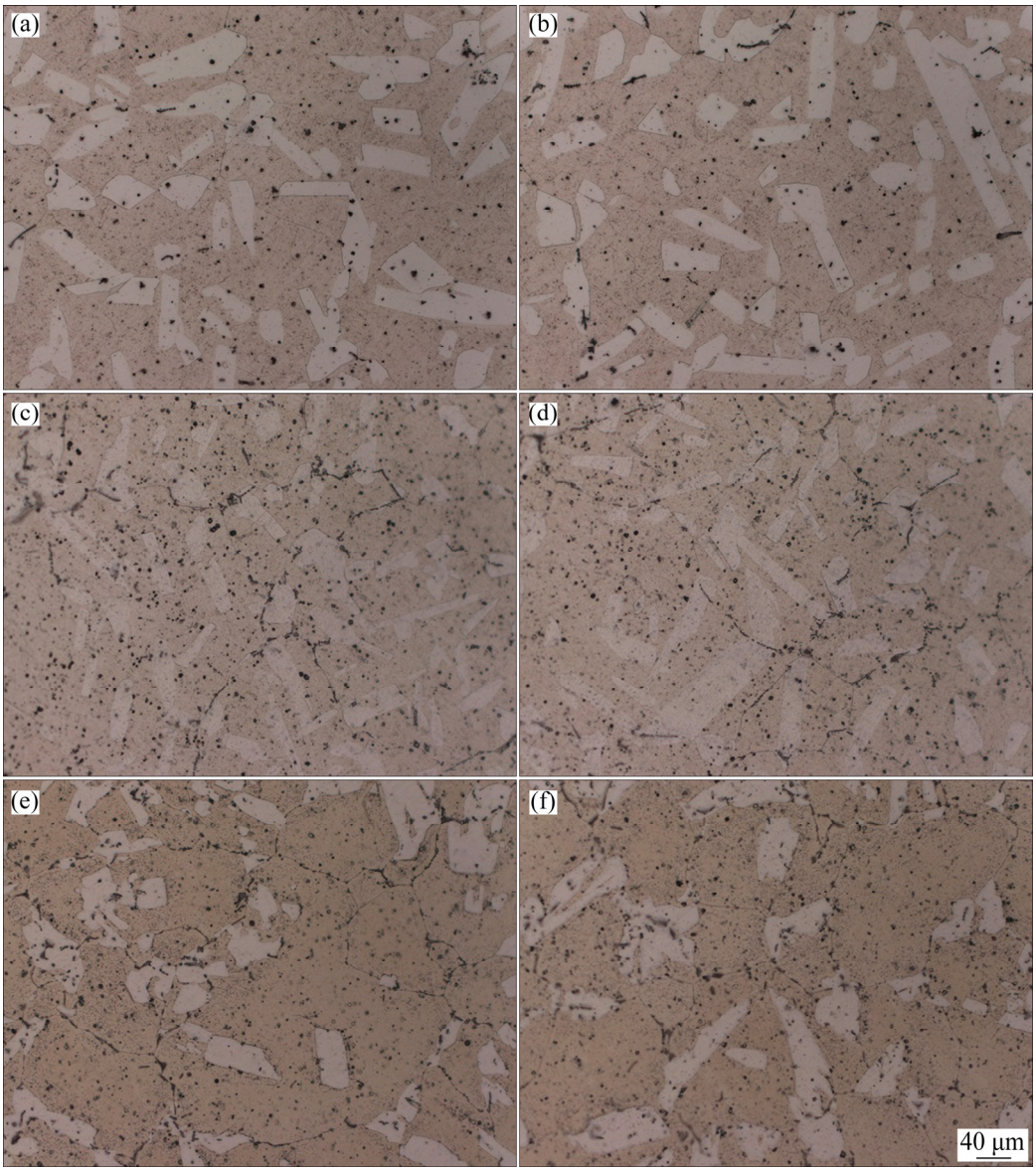

Fig. 11 Optical microstructures of LZG841 alloy after solution-treatment (350 °C, 4 h) and different aging treatments: (a) 75 °C, 1 h; (b) 125 °C, 1 h; (c) 75 °C, 4 h; (d) 125 °C, 4 h; (e) 75 °C, 256 h; (f) 125 °C, 256 h

the precipitate aggregating with the aging time increasing. The hardness of the solution-treated alloys with the aging treatment is prior to that of the as-cast alloys directly experiencing the aging treatment. The reason is that when Mg−Li alloys experience solid solution treatment, more Zn atoms dissolve into the matrix, and longer time is needed to transform from Li_2MgZn to LiMgZn phase. Though the hardness of LZG831 alloy is lower than that of LZG841 alloy in the aging process, decreasing level of hardness of LZG831 is less than that of LZG841 in aging process, which indicates that the thermostability of LZG831 is higher than that of LZG841. It can be explained that the volume fraction of precipitates in LZG841 is more than that of precipitates in LZG831, so second phases in LZG841 are more easily coarsened, which will weaken the effect of second phase strengthening.

4 Conclusions

(1) The microstructure of as-cast Mg−8Li−*x*Zn−*y*Gd (*x*=1, 2, 3, 4; *y*=1, 2; wt.%) alloys mainly consists of *α*-Mg phase, *β*-Li phase, *W*-phase, Mg−Li−Zn phase and Mg_3Gd phase. The morphology of *W*-phase is strip-like or net-like and that of Mg_3Gd phase presents block-like shape.

(2) For Mg−8Li−*x*Zn−1Gd (*x*=1, 2, 3, 4, wt.%) alloys, the volume fraction of *W*-phase increases while that of Mg_3Gd phase decreases with the increase of Zn content. The strength is improved with the increase of Zn

content, due to the second phase strengthening of fine strip-like *W*-phase and the solid solution strengthening of Zn element.

(3) For Mg−8Li−4Zn−*y*Gd (*y*=1, 2, wt.%) alloys, with the increase of Gd content, the *W*-phases aggregate and coarsen. The strength decreases with the increase of Gd content, which is ascribed to the stress concentration in coarse net-like *W*-phase.

(4) The as-cast Mg−8Li−4Zn−1Gd alloy exhibits the maximal ultimate tensile strength and yield strength of 197.0 MPa and 154.7 MPa, respectively.

(5) The peak aging of the tested alloys takes place at aging time around 4 h. LZG831 alloy exhibits higher thermostability than LZG841 alloy.

References

[1] WANG Qing-feng, LIU Ke, WANG Zhao-hui, LI Shu-bo, DU Wen-bo. Microstructure, texture and mechanical properties of as-extruded Mg−Zn−Er alloys containing W-phase [J]. Journal of Alloys and Compounds, 2014, 602: 32−39.

[2] XU D K, ZU T T, YIN M, XU Y B, HAN E H. Mechanical properties of the icosahedral phase reinforced duplex Mg−Li alloy both at room and elevated temperatures [J]. Journal of Alloys and Compounds, 2014, 582: 161−166.

[3] WEI Guo-bing, PENG Xiao-dong, ZHANG Bao, HADADZADEH A, XU Tian-cai, XIE Wei-dong. Influence of *I*-phase and *W*-phase on microstructure and mechanical properties of Mg−8Li−3Zn alloy [J]. Transactions of Nonferrous Metals Society of China, 2015, 25: 713−720.

[4] ZHANG Yang, ZHANG Jie, WU Guo-hua, LIU Wen-cai, ZHANG Liang, DING Wen-jiang. Microstructure and tensile properties of as-extruded Mg−Li−Zn−Gd alloys reinforced with icosahedral quasicrystal phase [J]. Materials and Design, 2015, 66: 162−168.

[5] ZHAO Jiong, ZHANG Jie, LIU Wen-cai, WU Guo-hua, ZHANG Liang. Effect of Y content on microstructure and mechanical properties of as-cast Mg−8Li−3Al−2Zn alloy with duplex structure [J]. Materials Science and Engineering A, 2016, 650: 240−247.

[6] MISHRA R K, GUPTA A K, RAO P R, SACHDEV A K, KUMAR A M, LUO A A. Influence of cerium on the texture and ductility of magnesium extrusions [J]. Scripta Materialia, 2008, 59: 562−565.

[7] MEI Jun, LIU Wen-cai, WU Guo-hua, ZHANG Yang, ZHANG Yi-tao, HONG Yi-kai, ZHANG Ruo-xi, XIAO L, DING Wen-jiang. Effect of complex melt-refining treatment on microstructure and mechanical properties of sand-cast Mg−10Gd−3Y−0.5Zr alloy [J]. Transactions of Nonferrous Metals Society of China, 2015, 25: 1811−1821.

[8] FENG Shi, LIU Wen-cai, ZHAO Jiong, WU Guo-hua, ZHANG Hao-hao, DING Wen-jiang. Effect of extrusion ratio on microstructure and mechanical properties of Mg−8Li−3Al−2Zn−0.5Y alloy with duplex structure [J]. Materials Science and Engineering A, 2017, 692: 9−16.

[9] SUN Yue-hua, WANG Ri-chu, PENG Chao-qun, FENG Yan, YANG Ming. Corrosion behavior and surface treatment of superlight Mg−Li alloys [J]. Transactions of Nonferrous Metals Society of China, 2017, 27: 1455−1475.

[10] POLLOCK T M. Weight loss with magnesium alloys [J]. Science, 2010, 328: 986−987.

[11] DING Hong-bo, LIU Qiang, ZHOU Hai-tao, ZHOU Xiao, ATRENS A. Effect of thermal-mechanical processing on microstructure and mechanical properties of duplex-phase Mg−8Li−3Al−0.4Y alloy [J]. Transactions of Nonferrous Metals Society of China, 2017, 27: 2587−2597.

[12] YANG Wen-peng, GUO Xue-feng. High strength magnesium alloy with *α*-Mg and *W*-phase processed by hot extrusion [J]. Transactions of Nonferrous Metals Society of China, 2011, 21: 2358−2364.

[13] LIU S J, YANG G Y, LUO S F, JIE W Q. Microstructure and mechanical properties of sand mold cast Mg−4.58Zn−2.6Gd−0.18Zr magnesium alloy after different heat treatments [J]. Journal of Alloys and Compounds, 2015, 644: 846−853.

[14] LIU Ke, ZHANG Jing-huai, LU Hua-yi, TANG Ding-xiang, ROKHLIN L L, ELKIN F M, MENG Jian. Effect of the long periodic stacking structure and W-phase on the microstructures and mechanical properties of the Mg−8Gd−Zn−0.4Zr alloys [J]. Materials and Design, 2010, 31: 210−219.

[15] HALILOVA H. Effect of additional elements on heat treatment characteristics and mechanical properties of superlight Mg−Li−Al alloys [J]. J Japan Inst Light Metals, 1997, 47: 195−201.

[16] ZHAO Jiong, LI Zhong-quan, LIU Wen-cai, ZHANG Jie, ZHANG Liang, TIAN Ying, WU Guo-hua. Influence of heat treatment on microstructure and mechanical properties of as-cast Mg−8Li−3Al−2Zn−*x*Y alloy with duplex structure [J]. Materials Science and Engineering A, 2016, 669: 87−94.

[17] LIU Yong, YUAN Guang-yin, ZHANG Song, ZHANG Xin-ping, LU Chen, DING Wen-jiang. Effects of Zn/Gd ratio and content of Zn, Gd on phase constitutions of Mg alloys [J]. Materials Transactions, 2008, 49: 941−944.

[18] MA Chun-jiang, LIU Man-ping, WU Guo-hua, DING Wen-jiang, ZHU Yan-ping. Tensile properties of extruded ZK60–RE alloys [J]. Materials Science and Engineering A, 2003, 349: 207−212.

[19] LIU Yong, YUAN Guang-yin, LU Chen, DING Wen-jiang. Stable icosahedral phase in Mg−Zn−Gd alloy [J]. Scripta Materialia, 2006, 55: 919−922.

[20] SINGH A, WATANABE M, KATO A, TSAI A P. Microstructure and strength of quasicrystal containing extruded Mg−Zn−Y alloys for elevated temperature application [J]. Materials Science and Engineering A, 2004, 385: 382−396.

[21] JU Y L, KIM D H, LIM H K, KIM D H. Effects of Zn/Y ratio on microstructure and mechanical properties of Mg−Zn−Y alloys [J]. Materials Letters, 2005, 59: 3801−3805.

[22] M LLER A, GARC S G, PREZ P, ADEVA P. Grain refinement of Mg−Zn−Y alloy reinforced by an icosahedral quasicrystalline phase by severe hot rolling [J]. Journal of Alloys and Compounds, 2007, 443: L1−L5.

[23] HU Yao-bo, DENG Juan, ZHAO Chong, WANG Jing-feng, PAN Fu-sheng. Microstructure and mechanical properties of as-quenched Mg−Gd−Zr alloys [J]. Transactions of Nonferrous Metals Society of China, 2011, 21: 732−738.

[24] BIAN Li-ping, MENG Yu-pu, QICHI L E, LIANG Wei, ZHAO Xing-guo, XUE Jin-bo. Microstructure evolution and mechanical property of Mg−9Li−5Gd−1Zr alloy [J]. Hot Working Technology, 2013, 559: 364−370.

[25] WU Horng-yu, LIN Jia-yu, GAO Zhen-wei, CHEN Hung-wei. Effects of age heat treatment and thermomechanical processing on microstructure and mechanical behavior of LAZ1010 Mg alloy [J]. Materials Science and Engineering A, 2009, 523: 7−12.

[26] LI Hong-bin, YAO Guang-chun, GUO Zhi-qiang, LIU Yi-han, JI Hai-bin. Microstructure, mechanical properties and age-hardening of Mg−Li alloy sheets [J]. Transactions of Nonferrous Metals Society of China, 2006, 16: 1729−1731.

[27] BAE D H, KIM Y, KIM I J. Thermally stable quasicrystalline phase in a superplastic Mg−Zn−Y−Zr alloy [J]. Materials Letters, 2006, 60: 2190−2193.

铸态 Mg−8Li−*x*Zn−*y*Gd (*x*=1, 2, 3, 4; *y*=1, 2)合金的显微组织与力学性能

欧阳思杰[1,2]，刘文才[1,2]，吴国华[1,2]，冀 浩[1,2]，高占奎[1,2]，彭 翔[1,2]，李中权[3,4]，丁文江[1,2]

1. 上海交通大学 材料科学与工程学院 轻合金精密成型国家工程中心和金属基复合材料重点实验室，上海 200240；
2. 上海创新材料研究所，上海 200444；
3. 上海航天精密机械研究所，上海 201600；
4. 上海金属材料近净成形工程技术研究中心，上海 201600

摘 要：通过真空熔炼方法制备铸态 Mg−8Li−*x*Zn−*y*Gd (*x*=1, 2, 3, 4; *y*=1, 2; wt.%)合金，并对合金的显微组织和力学性能进行研究。结果表明：随着 Zn 含量的增加，*W* 相($Mg_3Zn_3Gd_2$)的体积分数增加，而 Mg_3Gd 相的体积分数减少。Mg−8Li−*x*Zn−1Gd 合金强度的提高是因为随着锌含量的增加，细小片状 *W* 相的第二相强化以及 Zn 的固溶强化。随着钆含量的增加，Mg−8Li−4Zn−*y*Gd 合金的强度降低，这是因为形成粗化和不连续网状的 *W* 相。Mg−8Li−4Zn−1G 合金表现出最优的综合性能，屈服强度为 154.7 MPa、抗拉强度为 197.0 MPa、伸长率为 12.4%。另外，对合金的时效行为进行研究。

关键词：Mg−Li−Zn−Gd 合金；*W* 相；显微组织；力学性能；时效行为

(Edited by Bing YANG)